THE JOURNAL OF PHYSICAL CHEMISTRY LETTERS
A JOURNAL OF THE AMERICAN CHEMICAL SOCIETY

pubs.acs.org/JPCL

Letter

Defect-Induced Transport Enhancement in Carbon–Boron Nitride–Carbon Heteronanotube Junctions

Laith A. Algharagholy and V. M. García-Suárez*

Cite This: *J. Phys. Chem. Lett.* 2023, 14, 2056–2064

Read Online

ACCESS | Metrics & More | Article Recommendations | Supporting Information

ABSTRACT: New heteromaterials, particularly those involving nanoscale elements such as nanotubes, have opened a wide window for the next generation of materials and devices. Here, we perform density functional theory (DFT) simulations combined with a Green's function (GF) scattering approach to investigate the electronic transport properties of defective heteronanotube junctions (hNTJs) made of (6,6) carbon nanotubes (CNT) with a boron nitride nanotube (BNNT) as scatterer. We used the sculpturene method to form different heteronanotube junctions with various types of defects in the boron nitride part. Our results show that the defects and the curvature induced by them have a nontrivial impact on the transport properties and, interestingly, lead to an increase of the conductance of the heteronanotube junctions compared to the free-defect junction. We also show that narrowing the BNNTs region leads to a large decrease of the conductance, an effect that is opposite to that of the defects.

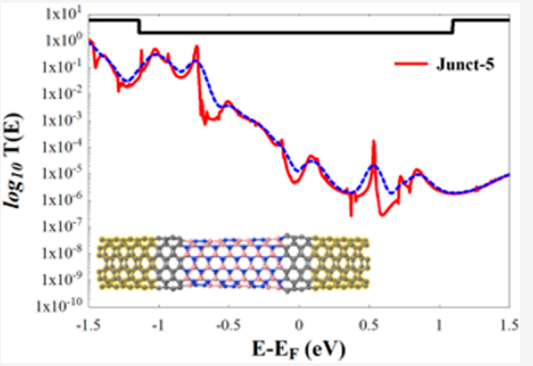

Since their discovery by Sumio Iijima in 1991,[1] carbon nanotubes (CNTs) have received tremendous research attention for their unique electronic,[2−5] mechanical,[5−7] optical,[8,9] and thermal[10−12] properties. Carbon nanotubes have different electronic behaviors; they can be semiconductors or conductors depending on the chirality, which is often difficult to control in synthesis.[13,14] Boron nitride nanotubes (BNNTs), on the other hand, which were first discovered in 1995,[15] exhibit a wide energy gap of approximately of 5 eV.[15,16] A variety of techniques can be used for manufacturing CNTs and BNNTs, such as arc discharge,[13,17−19] laser ablation,[20−22] and chemical vapor deposition (CVD),[23−25] which usually produce again a mixture of chiralities. Various research works have been undertaken on BNNT, which mainly focused on properties such as the electronic structure,[15,26,27] and optical,[28−30] thermal,[31,32] and mechanical[26,30,33] properties. Regarding the electronic structure, introducing defects in nanotubes has a nontrivial influence on their electronic structure,[34] e.g., defect-induced deformations in CNTs[35−38] lead to an extreme decrease in the electronic transport, whereas in BNNTs, defects[39−41] produce a narrow energy gap. The most common defects in nanotubes are five–seven (Stone–Wales) defects.[38,42−45] Previous studies including molecular dynamics (MD) calculations[46−50] reported that such defects are stable even at high temperatures. On the other hand, modulating the periodic structure of pristine CNTs by other materials such as nitrogen and boron to form heteronanotubes, can modify their electronic properties,[51−54] turning, for instance, a metallic CNT into a semiconductor.[52,54−57]

A variety of experimental techniques have confirmed the synthesis and characterization of nitrogen/boron-doped[58−63] CNTs. Heterojunctions, such as carbon–boron nitride heteronanotube junctions are also energetically stable[52,64,65] and have a conductance that can be tuned by altering the width of the boron nitride strips in the heteronanotube.[66] Despite many difficulties involved in the preparation of carbon–boron nitride heterojunctions, experimental efforts have successfully synthesized them using different methods.[67−72] In this work, we investigate the electronic transport properties of ideal heterojunctions consisting of (6,6) CNTs as left/right leads and a (6,6) BNNT as scattering region. We also consider the impact of different factors such as defects and the width of the scatterer (BNNT) on the transport properties.

To form the heteronanotube junctions (hNTJs) shown in Figure 1(b–g), we used the sculpturene method,[64] which provides a methodology for creating deterministic carbon nanotubes (CNTs) through the reconstruction of bilayered graphene nanoribbons (bi-GNRs), including bilayered heteronanoribbons materials, such as graphene (G) and boron nitride (BN). Notice that, even though the strain can be large and act as a destabilizing factor in the initial stages of the formation of

Received: January 1, 2023
Accepted: February 15, 2023
Published: February 16, 2023

https://doi.org/10.1021/acs.jpclett.3c00004
J. Phys. Chem. Lett. 2023, 14, 2056–2064

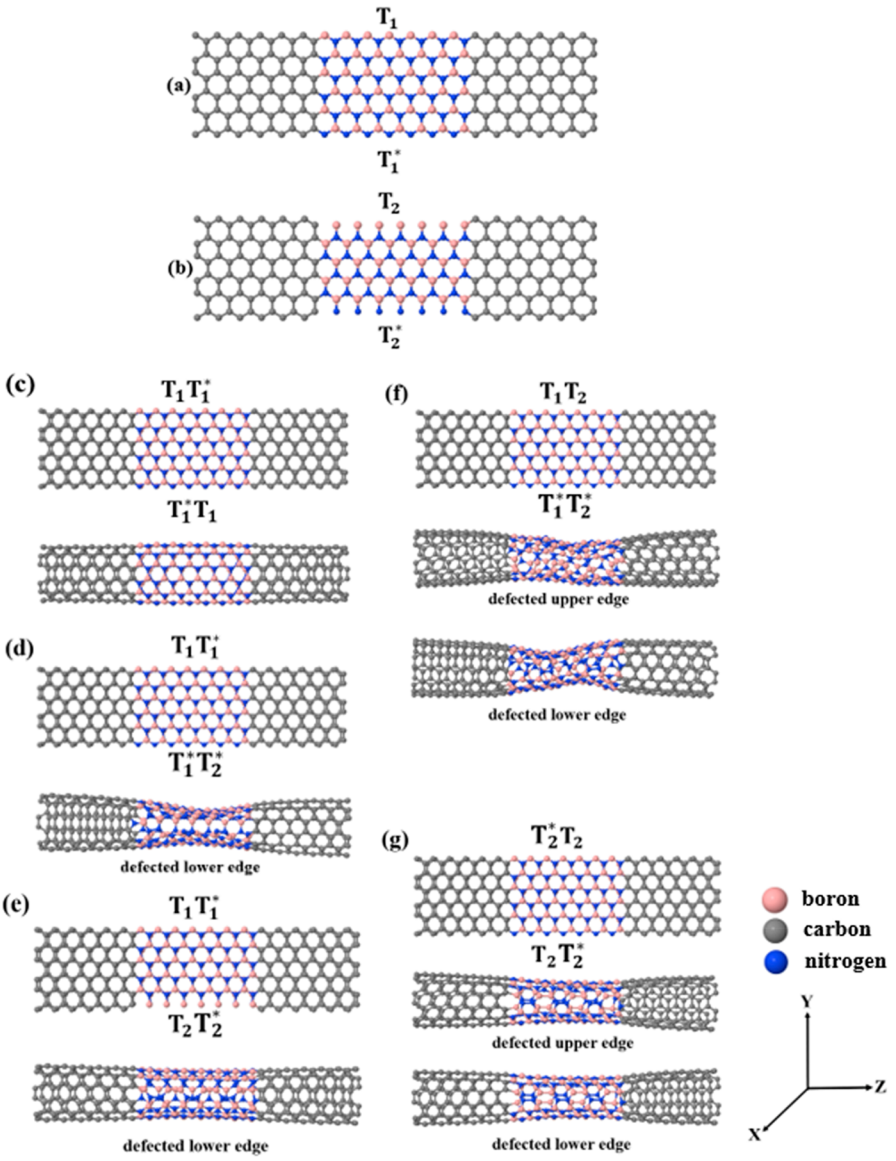

Figure 1. Single-layered zigzag hNRs with (a) T_1 termination and (b) T_2 termination. The top subfigures in figures (c−g) show the initial supercell obtained by cutting a zigzag AA-stacked bilayered hNRs, while the bottom subfigures show the relaxed sculpturenes, which make the CNT-BNNT-CNT heteronanotube junctions. Each figure corresponds to a different configuration of terminations: (c) with $T_1T_1^*$ (top upper/lower edges) and $T_1^*T_1$ termination (bottom upper/lower edges), (d) with $T_1T_1^*$ termination (top upper edge with T_1 termination and top lower edge with T_1^* termination), and $T_1^*T_2^*$ termination (bottom upper and lower edges terminated with T_1^* and T_2^*, respectively), (e) with $T_1T_1^*$ termination (top upper edge with T_1 termination and lower edge with T_1^* termination) and $T_2T_2^*$ termination (bottom upper edge with T_2 and lower edges with T_2^*), (f) with T_1T_2 termination (top upper/lower edges are terminated with T_1 and T_2 terminations respectively) and $T_1^*T_2^*$ termination (top upper edge is with T_1^* termination and bottom lower edge is with T_2^* termination), and (g) with $T_2^*T_2$ termination (top upper edge with T_1^* termination and bottom lower edge with T_2^* termination) and $T_2T_2^*$ termination (top upper edge terminated with T_2 termination and bottom lower edge terminated with T_2^* termination).

the nanotubes, the structures naturally evolve to such configurations after several relaxation steps, provided the initial ribbons are close enough to each other. This procedure opens a wide window of options for constructing topologically unique nanostructures. In this work, we started with AA-staked zigzag bilayered heteronanoribbons (bi-hNRs), each layer composed of graphene-boron nitride-graphene (G-BN-G), to form hNTJs, which consist of (6,6) CNTs as left/right leads and a boron nitride nanotube (BNNT) as scatterer (CNT-BNNT-CNT). To optimize the initial supercells (AA-staked zigzag bi-hNRs), we employed the SIESTA[73] implementation of density functional theory (DFT). We used the local density approximation (LDA)[74] with the Ceperley−Alder (CA) exchange correlation functional, and double-ζ polarized (DZP) basis sets of pseudoatomic orbitals, together with norm-conserving pseudopotentials. Notice that the LDA usually overestimates the binding, giving distances between atoms a bit smaller than the real ones, but works properly in general to describe van der Waals interactions[75] such as those present in the initial stages of the design of the sculpturenes. The initial supercells were relaxed until all the forces were smaller than 0.005 eV/Å. To avoid the interaction between neighboring heterostructures, a vacuum space of 50 Å was included along the X and Y directions, whereas along the Z direction the structures were periodic. For the leads calculations, a k-point grid of 1 × 1 × 30 in the Brillouin

https://doi.org/10.1021/acs.jpclett.3c00004
J. Phys. Chem. Lett. 2023, 14, 2056−2064

Table 1. Number and Types of Defects That Emerge in Each of the Relaxed hNTJs

Junction	Edge	Type of ring					Number of defects
		Square	Pentagon	Heptagon	Octagon	Nonagon	
Junct-2	bottom	---	**5 rings** 2 B atoms 3 N atoms	**2 rings** 2 B atoms 2 N atoms 2 C atoms	---	---	5 pentagons 2 heptagons
Junct-3	bottom	**1 ring** 1 B atoms 1 N atoms 2 C atoms	**1 ring** 2 B atoms 1 N atoms 2 C atoms **3 rings** 3 B atoms 2 N atoms **3 rings** 2 B atoms 3 N atoms	**3 rings** 3 B atoms 4 N atoms **3 rings** 4 B atoms 3 N atoms	---	**1 ring** 2 B atoms 2 N atoms 4 C atoms	1 square 7 pentagons 6 heptagons 1 nonagon
Junct-4	top	**1 ring** 3 B atoms 1 N atoms	**1 rings** 4 B atoms 1 N atoms **1 rings** 2 B atoms 1 N atoms 2 C atoms **2 rings** 3 B atoms 2 N atoms	---	**4 rings** 5 B atoms 3 N atoms	---	1 square 4 pentagons 4 octagons
	bottom	---	**1 ring** 1 N atoms 4 C atoms **1 ring** 1 B atoms 4 N atoms **1 ring** 1 B atoms 2 N atoms 2 C atoms **3 rings** 2 B atoms 3 N atoms	**3 rings** 3 B atoms 4 N atoms	**1 ring** 3 B atoms 5 N atoms **1 ring** 2 B atoms 4 N atoms 2 C atoms	---	5 pentagons 3 heptagons 2 nonagon
Junct-5	top	**1 ring** 1 B atoms 1 N atoms 2 C atoms	**1 ring** 2 B atoms 1 N atoms 2 C atoms **3 rings** 3 B atoms 2 N atoms **3 rings** 2 B atoms 3 N atoms	**3 rings** 3 B atoms 4 N atoms **3 rings** 4 B atoms 3 N atoms	---	**1 ring** 2 B atoms 2 N atoms 5 C atoms	1 square 7 pentagons 6 heptagons 1 nonagon
	bottom	**same as top**	**same as top**	**same as top**	**same as top**	**same as top**	

zone was used. Once the final hNTJs were achieved, we took the mean field Hamiltonian (MFH) and overlap matrices from SIESTA, and, using the GOLLUM[76] implementation of equilibrium transport theory, we calculated the low bias electron transmission coefficients $T(E)$ and currents I.

For single-layered zigzag hNRs, there are four possible side edges of the BN region, as shown in Figure 1(a,b). We name these terminations as T_1, T_1^*, T_2, and T_2^*. In an ideal case, the upper/lower edges in the boron nitride region would have the T_1 and T_1^* configurations (Figure 1a). The T_2 termination is created by eliminating a complete row of nitrogen atoms, while the T_2^* termination is obtained after removing a complete row of boron atoms. Note that in the presence of T_2 and T_2^* terminations, shown in Figure 1b, the resulting hNTJs will have a defected BNNT region or scatterer (see below).

We conveniently refer from now on to the hNTJs shown in Figure 1(c–g) as Junct-1, Junct-2, Junct-3, Junct-4, and Junct-5, respectively. For more clarity, Figure S1 (Supporting Information) schematically shows the defects created in the relaxed BNNT (scatterer) of the hNTJs displayed in Figure 1(d–g). From Figure S1, we can see that a variety of defects with different geometries arise in the resulting hNTJs (Junct-2, Junct-3, Junct-4, and Junct-5) when the sculpturenes are made. Junct-2 and Junct-3 are relaxed with one defected side (bottom), while Junct-4 and Junct-5 are relaxed with a top/bottom defected side. Table 1 summarizes the type and number of defects shown in Figure S1. From this table, we can see that the total number defects in Junct-2, Junct-3, Junct-4, and Junct-5 are 7, 15, 19, and 30, respectively. Figure 2 shows the five hNTJs. The yellow shaded region represents the left/

https://doi.org/10.1021/acs.jpclett.3c00004
J. Phys. Chem. Lett. 2023, 14, 2056−2064

right (6,6) CNT leads, while the middle region is the extended molecule including the BNNT.

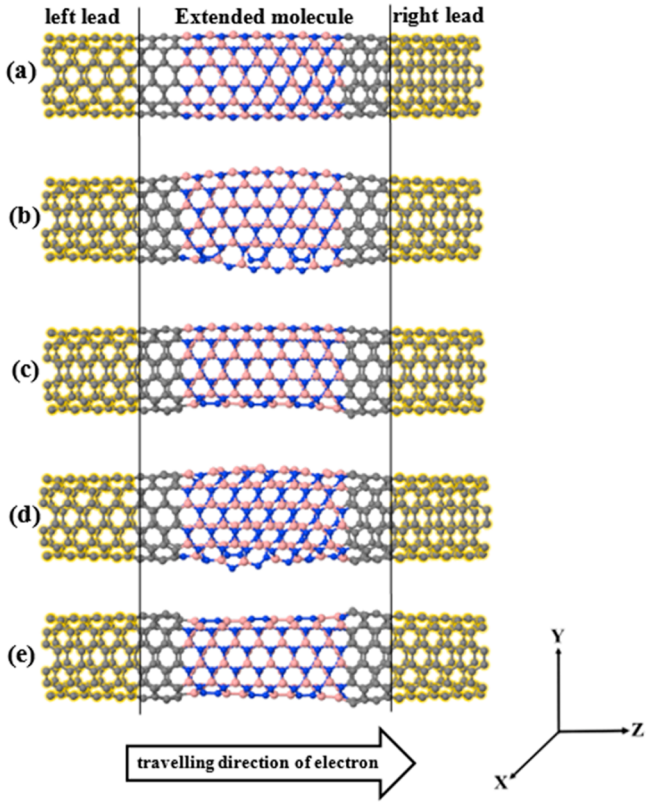

Figure 2. (a) Ideal Junct-1, (b−e) defected Junct-2, Junct-3, Junct-4, and Junct-5, respectively. All junctions are periodic in the *Z*-direction, and finite in the *X* and *Y* directions.

In what follows, we investigate the transmission coefficient $T(E)$ of the hNTJs shown in Figure 2, which are plotted in Figure 3. The black line in the subfigures of Figure 3 represents the $T(E)$ from the left lead to the right lead in the absence of the extended molecule (i.e., an ideal (6,6) CNT), which, according to the Landauer description, is equal to the number of open channels (NOC), since these structures (leads) are periodic in the Z direction.[55] From the same figure we can see that the $T(E)$ of the hNTJs is obviously inhibited due to the presence of the BNNT. Notice also that Junc-1 is not periodic, since it has the BNNT scatterer, but it is free of defects. However, contrary to what one would expect, the defected hNTJs show in general (specially at the original Fermi level given by DFT) higher conductances than the defect-free Junct-1. This result, which it is a somewhat surprising behavior that ensues from the fact that the defect-free system is highly insulating, can be explained by the increase of electron delocalization generated by the emergence of dangling bonds at the defects (see below).

From Figure 3, we can also see that there is a relationship between the geometry of hNTJs and the conductance. It is worth mentioning here that in the case of two tubes being linked symmetrically, the formed junction has no bend[77] as we see in the BNNT region of Junct-1 (Figure 2a), whereas the hNTJs shown in Figure 2(b−e) present curved BNNTs. These curvatures are due to the existence of the defects, which agrees with previous published works.[77−80] Previous research reported that defects, not only pentagon (five-atom ring) and heptagon (seven-atom ring), lead to bend the nanotubes with different angles, and also tune the electric properties of the nanotubes.[81−86] Note that sharp bends in CNTs and BNNTs have been observed.[26,80,81,87−89] BNNTs,[83,90] which are perfect insulators, might be turned to semiconductors (reduce the energy gap) by bending the tubular structure. Having a look at Figure 1, it is clear that Junct-2 and Junct-4 shown in Figure 1(d,f) have the most curved BNNTs compared to the BNNTs in the rest of hNTJs in Figure 1. These hNTJs (Junct-2 and Junct-4) show the highest conductance as seen in Figure 3(b,d), and this improvement in conductance is not only due to of the existence of the defects, but also due to the curvatures that are created because of the formed defects in the BNNTs regions. Indeed, by assigning topological numbers to local changes in defects with respect to the hexagonal curvature, i.e., pentagons, +1; squares, +2; heptagons, −1; octagons, −2; and nonagons, −3; we can see that the total induced curvatures in each junction are the following: Junct-2, +3; Junct-3, 0; Junct-4, top edge, −2, bottom edge, −4; Junct-5, top and bottom edge, 0. This relates again the enhancement of conductance of Junct-2 and Junct-4 to the curvature. The LDOS calculations in Figure S2(b,d) also show that Junct-2 and Junct-4 have the highest delocalized states around the curvatures and defects, which further confirms the previous claims.

To provide another evidence of the transport enhancement, we calculate the maximum current (I) of the hNTJs, shown in Figure 2(a−e) at room temperature for a small finite voltage using the following equation:[91]

$$I = \frac{q_e}{h}\int \mathrm{d}E T(E)(f(E-\mu_{LL}) - f(E-\mu_{RL})) \quad (1)$$

where $q_e = |q_e|$ is the electron charge, h is Planck's constant, $T(E)$ is the electronic transmission coefficient calculated with GOLLUM, f is Fermi−Dirac distribution function, $f(E-\mu) = 1/(1 + e^{(E-\mu)/K_BT})$, with μ_{LL} and μ_{RL} being the electrochemical potentials of the left lead and right lead, respectively, and T is the temperature. The resulting currents are shown in Figure 4.

Once again, Figure 4 shows that there is in general an increase in the current of the hNTJs with more defects shown in Figure 2(b−e), compared to the ideal Junct-1. This increase is due to the presence of defects in the BNNT, which improve the transmission of the junction as compared to that of the insulating BNNT without defects. Notice, however, that the smallest current in most of the bias window is that of Junct-3. The current of Junct-4 can also be smaller than that of Junct-1 in some bias ranges. These two last junctions are characterized by the presence of a somewhat periodic array of defects, which seems to preserve also to a great extent the insulating behavior of the BNNT part. Notice as well that the current of Junct-1 is almost equal to that of Junct-5 in most of the bias range, which is due to the similarity between both junctions, since Junct-5 is equivalent to Junct-1 with two less rows of atoms at the top and bottom edges. Finally, in terms of current, the best junction is Junct-2.

Apart from defects and curvature, another factor that can greatly influence the transport properties is the width of the scattering region. Narrower BN regions can be built again with the sculpturene method, as can be seen in Figure 5. Figure 5a shows the AA-staked zigzag bi-hNRs displayed in Figure 1c (top subfigure) after eliminating a complete row of the boron and nitrogen atoms from the upper edges of the top AA-staked zigzag bi-hNRs and the lower edges of the bottom AA-staked

https://doi.org/10.1021/acs.jpclett.3c00004
J. Phys. Chem. Lett. 2023, 14, 2056−2064

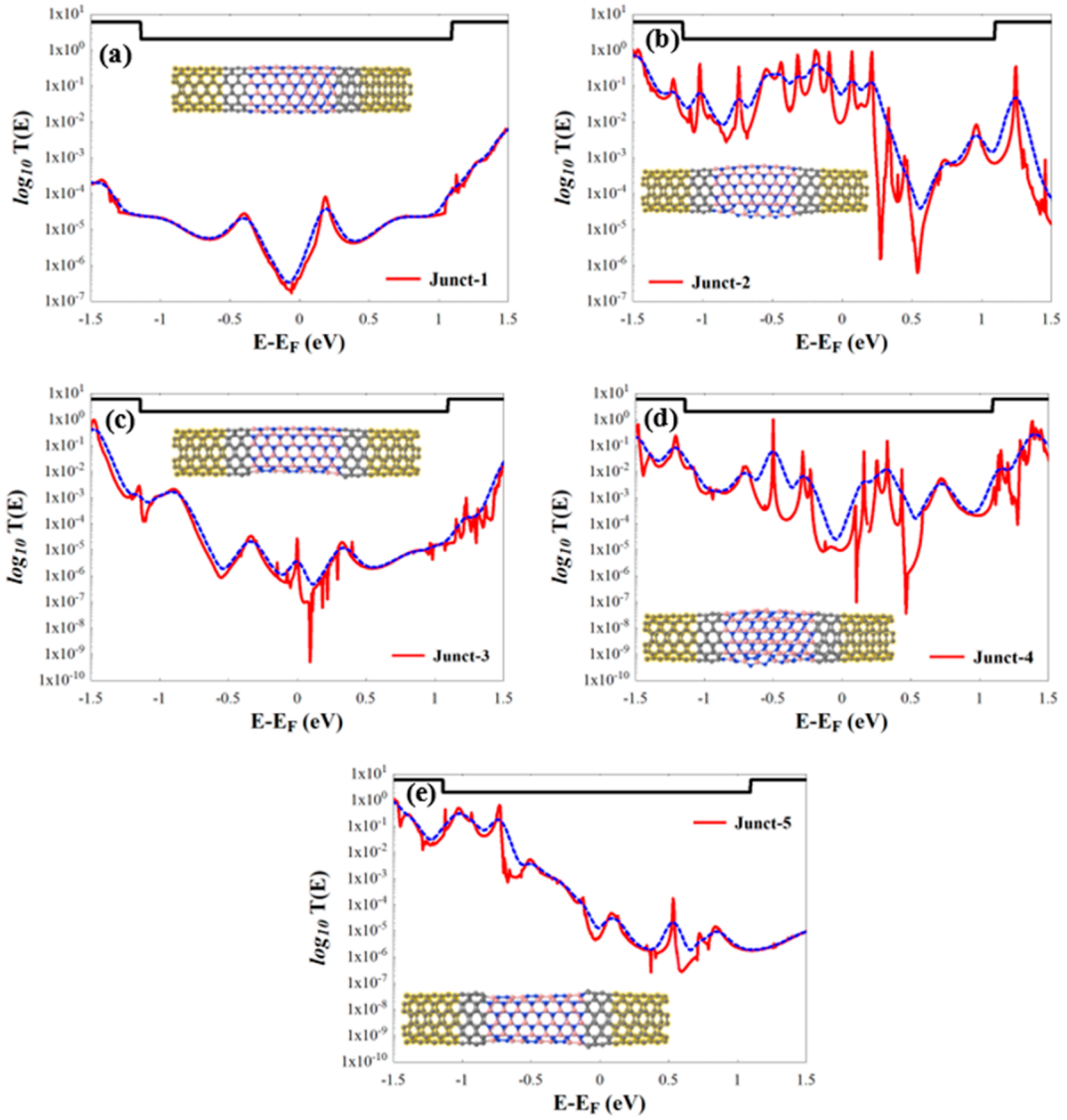

Figure 3. (a–e) $T(E)$ of the hNTJs shown in Figure 2(a–e), respectively. The dotted blue line in all subfigures shows the conductance at room temperature (T = 300 K) and the insets represent the hNTJs. E_F is the predicted Fermi energy value given by DFT, and it shifted to zero.

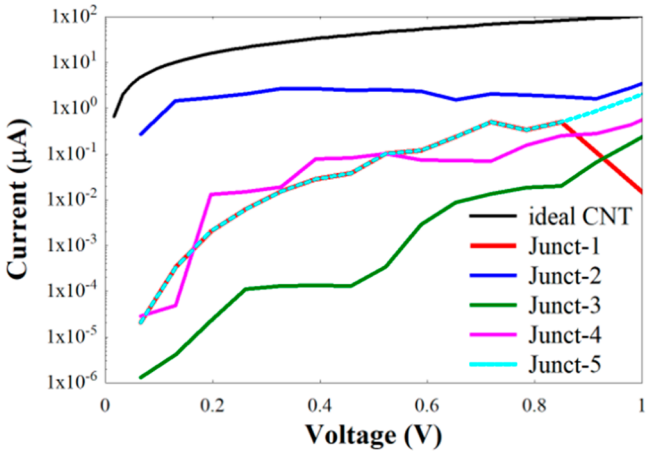

Figure 4. Currents of the hNTJs displayed in Figure 2(a–e).

zigzag bi-hNRs. We repeated the same strategy with the initial supercell shown in Figure 5b by removing completely two rows of the boron and nitrogen atoms. Later, we let them relax to form the hNTJs shown in Figure 5(c,d). We call these junctions with narrower BN regions Junct-6 and Junct-7, respectively.

Figure 5c shows that the middle region (BN) of Figure 5a is finally relaxed into a (4,4) BNNT, whereas the middle BN region of Figure 5b relaxes into a bridge of multichains composed of boron and nitrogen atoms, as can be seen in Figure 5d (side view) and Figure 5e (top view). Figure 6 shows the resulting $T(E)$ and currents of Junct-6 and Junct-7. As can be seen, there is an extreme drop of the conductance compared to the conductance of the hNTJs shown in Figure 2, i.e., as the width of the BN region is reduced, the conductance of the hNTJs decreases.

For a deeper understanding of the evolution of the conductance and current of the heterojunctions shown in Figure 2 and Figure 5, we calculated the Local Density of States (LDOS) in an energy window around E_F, from −0.1 eV to +0.1 eV, as shown in Figure S2. From this figure it is clear that the defects in Junct-2 and Junct-4 give rise to more delocalized states around the E_F, leading to possible paths through which the electrons can travel more easily, whereas the

https://doi.org/10.1021/acs.jpclett.3c00004
J. Phys. Chem. Lett. 2023, 14, 2056−2064

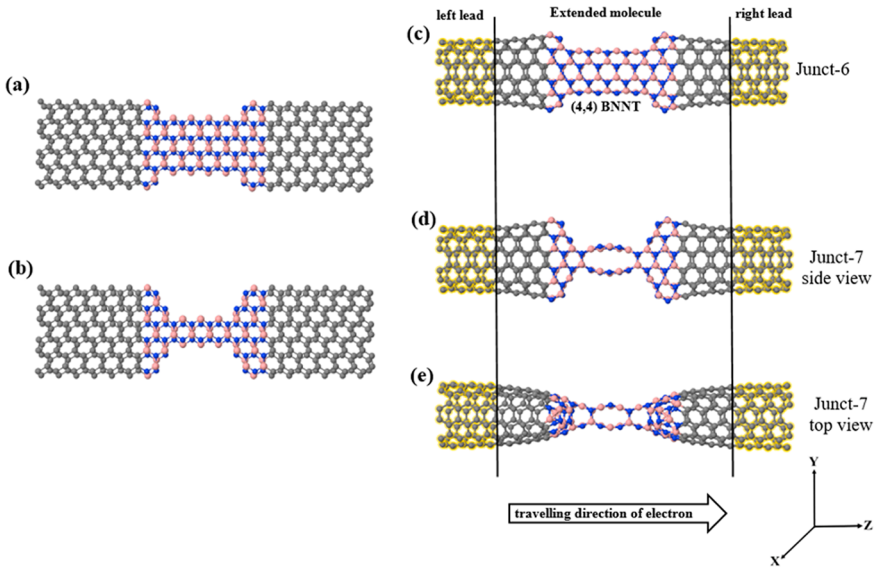

Figure 5. (a,b) Initial zigzag AA-staked bi-hNRs, (c,d) the obtained hNTJs (Junct-6 and Junct-7) after relaxing the initial supercells in (a,b), and (e) top view of Junct-7 shown in (d). The yellow shaded region shown in (c−e) is the (6,6) CNT as left and right leads. All structures are infinite in the Z direction and finite in the X and Y directions.

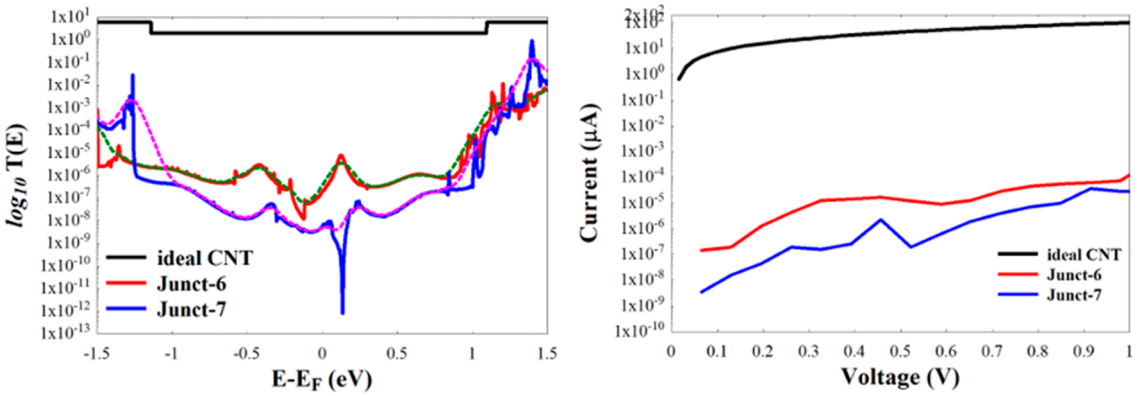

Figure 6. $T(E)$ (left) and current (right) of Junct-6 and Junct-7 shown in Figure 5(c,d). The dotted lines in the left subfigure shows the conductance calculated at room temperature of Junct-6 and Junct-7.

defects in the rest of the heterojunctions (Junct-1, Junct-3, Junct-5, Junct-6, and Junct-7) do not give additional states in the BN part around E_F, keeping the central part roughly insulating. This explains then the enhancement in conductance and current of Junct-2 and Junct-4.

Additionally, we note that resonances that appear around E_F in $T(E)$ should lead to enhancement of the Seebeck coefficient (S) of the hNTJs. To demonstrate this, we calculate S for all hNTJs, shown in Figure S3. The obtained values of S, listed in Table S1, are remarkable and illustrate again that hNTJs in contact with ideal CNTs can lead to a rather good thermoelectric performance. More research would be needed in any case to further demonstrate the enhancement in the thermoelectric properties of the hNTJs, which is not the main target of this work.

Conclusions: In this work, we have investigated the electronic and transport properties of defects that might be created in hNTJs using the sculpturene method, or manufactured by other methods, and the influence of other factors such as the curvature induced by the defects. Our results show that the transmission from left lead to right lead through the defective BNNTs is significantly reduced compared with that for ideal CNTs. On the other hand, the presence of defects and the induced curvature lead to an enhancement in the conductance of hNTJs, compared to that of the free-defect hNTJ. We also demonstrated that narrowing the BNNT region leads to remarkable decreases of the conductance. Our LDOS analysis explains the high transmission of Junct-2 and Junct-4, which show highly delocalized states around E_F, while for the other hNTJs, shows no evidence of such states in the scattering region. Furthermore, our findings demonstrate that defects give rise to improvements in the Seebeck coefficient (S) of the hNTJs. This work lays then the foundation for the design of nanoscale sensors that, through the change in their transport properties, can act as detectors of particles that generate defects in materials.

■ ASSOCIATED CONTENT

Data Availability Statement

The data that support the findings of this study are available from the corresponding author upon reasonable request.

Supporting Information

The Supporting Information is available free of charge at https://pubs.acs.org/doi/10.1021/acs.jpclett.3c00004.

https://doi.org/10.1021/acs.jpclett.3c00004
J. Phys. Chem. Lett. 2023, 14, 2056−2064

Additional analysis and calculations, including a figure with the types of defects and calculations of the local density of states and the Seebeck coefficients (PDF)
Transparent Peer Review report available (PDF)

AUTHOR INFORMATION

Corresponding Author

V. M. García-Suárez − *Departamento de Física, Universidad de Oviedo & CINN, Oviedo 33007, Spain;* orcid.org/0000-0002-7392-4648; Email: vm.garcia@cinn.es, garciavictor@uniovi.es

Author

Laith A. Algharagholy − *Department of Physics, College of Science, University of Sumer, Al Rifaee 64005 Thi-Qar, Iraq*

Complete contact information is available at: https://pubs.acs.org/10.1021/acs.jpclett.3c00004

Notes

The authors declare no competing financial interest.

ACKNOWLEDGMENTS

Laith A. Algharagholey acknowledges the Iraqi Ministry of Higher Education and Scientific Research and University of Sumer for the support. V. M. García-Suárez thanks the Spanish Ministerio de Ciencia, Innovación y Universidades for funding through the project PGC2018-094783−B-I00.

REFERENCES

(1) Iijima, S. Helical microtubules of graphitic carbon. *nature* **1991**, *354*, 56−58.
(2) Odom, T. W.; Huang, J.-L.; Kim, P.; Lieber, C. M. Structure and electronic properties of carbon nanotubes. *J. Phys. Chem. B* **2000**, *104*, 2794−2809.
(3) Fischer, J. E.; Johnson, A. T. Electronic properties of carbon nanotubes. *Curr. Opin. Solid State Mater. Sci.* **1999**, *1*, 28−33.
(4) Issi, J.-P.; Langer, L.; Heremans, J.; Olk, C. Electronic properties of carbon nanotubes: experimental results. *Carbon* **1995**, *33*, 941−948.
(5) Prylutskyy, Y. I.; Durov, S.; Ogloblya, O.; Buzaneva, E.; Scharff, P. Molecular dynamics simulation of mechanical, vibrational and electronic properties of carbon nanotubes. *Comput. Mater. Sci.* **2000**, *17*, 352−355.
(6) Salvetat, J.-P.; Bonard, J.-M.; Thomson, N.; Kulik, A.; Forro, L.; Benoit, W.; Zuppiroli, L. Mechanical properties of carbon nanotubes. *Appl. Phys. A: Mater. Sci. Process.* **1999**, *69*, 255−260.
(7) Ruoff, R. S.; Qian, D.; Liu, W. K. Mechanical properties of carbon nanotubes: theoretical predictions and experimental measurements. *Comptes Rendus Physique* **2003**, *4*, 993−1008.
(8) Wan, X.; Dong, J.; Xing, D. Optical properties of carbon nanotubes. *Phys. Rev. B* **1998**, *58*, 6756.
(9) Kataura, H.; Kumazawa, Y.; Maniwa, Y.; Umezu, I.; Suzuki, S.; Ohtsuka, Y.; Achiba, Y. Optical properties of single-wall carbon nanotubes. *Synthetic metals* **1999**, *103*, 2555−2558.
(10) Hone, J.; Llaguno, M.; Biercuk, M.; Johnson, A.; Batlogg, B.; Benes, Z.; Fischer, J. Thermal properties of carbon nanotubes and nanotube-based materials. *Applied physics A* **2002**, *74*, 339−343.
(11) Hone, J. Carbon nanotubes: thermal properties. *Dekker Encyclopedia of Nanoscience and nanotechnology* **2004**, *7*, 603−610.
(12) Xu, Y.; Zhang, Y.; Suhir, E.; Wang, X. Thermal properties of carbon nanotube array used for integrated circuit cooling. *J. Appl. Phys.* **2006**, *100*, 074302.
(13) Ebbesen, T. W.; Ajayan, P. M. Large-scale synthesis of carbon nanotubes. *Nature* **1992**, *358*, 220−222.
(14) Lan, Y.; Wang, Y.; Ren, Z. Physics and applications of aligned carbon nanotubes. *Adv. Phys.* **2011**, *60*, 553−678.
(15) Chopra, N. G.; Luyken, R.; Cherrey, K.; Crespi, V. H.; Cohen, M. L.; Louie, S. G.; Zettl, A. Boron nitride nanotubes. *science* **1995**, *269*, 966−967.
(16) Golberg, D.; Bando, Y.; Huang, Y.; Terao, T.; Mitome, M.; Tang, C.; Zhi, C. Boron nitride nanotubes and nanosheets. *ACS Nano* **2010**, *4*, 2979−2993.
(17) Tiano, A. L.; Park, C.; Lee, J. W.; Luong, H. H.; Gibbons, L. J.; Chu, S.-H.; Applin, S.; Gnoffo, P.; Lowther, S.; Kim, H. J. Boron nitride nanotube: synthesis and applications. *Proc. SPIE 9060, Nanosensors, Biosensors, and Info-Tech Sensors and Systems 2014* **2014**, No. 2045396, DOI: 10.1117/12.2045396.
(18) Journet, C.; Maser, W.; Bernier, P.; Loiseau, A.; de La Chapelle, M. L.; Lefrant, d. S.; Deniard, P.; Lee, R.; Fischer, J. Large-scale production of single-walled carbon nanotubes by the electric-arc technique. *nature* **1997**, *388*, 756−758.
(19) Thostenson, E. T.; Ren, Z.; Chou, T.-W. Advances in the science and technology of carbon nanotubes and their composites: a review. *Composites science and technology* **2001**, *61*, 1899−1912.
(20) Hornbostel, B.; Haluska, M.; Cech, J.; Dettlaff, U.; Roth, S. Arc discharge and laser ablation synthesis of singlewalled carbon nanotubes. *Carbon Nanotubes* **2006**, 1−18, DOI: 10.1007/1-4020-4574-3_1.
(21) Kuo, T.; Chi, C.; Lin, I. Synthesis of carbon nanotubes by laser ablation of graphites at room temperature. *Jpn. J. Appl. Phys.* **2001**, *40*, 7147.
(22) Golberg, D.; Bando, Y.; Eremets, M.; Takemura, K.; Kurashima, K.; Yusa, H. Nanotubes in boron nitride laser heated at high pressure. *Appl. Phys. Lett.* **1996**, *69*, 2045−2047.
(23) Bhaviripudi, S.; Mile, E.; Steiner, S. A.; Zare, A. T.; Dresselhaus, M. S.; Belcher, A. M.; Kong, J. CVD synthesis of single-walled carbon nanotubes from gold nanoparticle catalysts. *J. Am. Chem. Soc.* **2007**, *129*, 1516−1517.
(24) Qiu, J.; An, Y.; Zhao, Z.; Li, Y.; Zhou, Y. Catalytic synthesis of single-walled carbon nanotubes from coal gas by chemical vapor deposition method. *Fuel processing technology* **2004**, *85*, 913−920.
(25) Lourie, O. R.; Jones, C. R.; Bartlett, B. M.; Gibbons, P. C.; Ruoff, R. S.; Buhro, W. E. CVD growth of boron nitride nanotubes. *Chem. Mater.* **2000**, *12*, 1808−1810.
(26) Vaccarini, L.; Goze, C.; Henrard, L.; Hernandez, E.; Bernier, P.; Rubio, A. Mechanical and electronic properties of carbon and boron−nitride nanotubes. *Carbon* **2000**, *38*, 1681−1690.
(27) Zhang, Z.; Guo, W.; Dai, Y. Stability and electronic properties of small boron nitride nanotubes. *J. Appl. Phys.* **2009**, *105*, 084312.
(28) Oku, T.; Koi, N.; Suganuma, K. Electronic and optical properties of boron nitride nanotubes. *J. Phys. Chem. Solids* **2008**, *69*, 1228−1231.
(29) Chen, R. B.; Shyu, F. L.; Chang, C. P.; Lin, M. F. Optical properties of boron nitride nanotubes. *J. Phys. Soc. Jpn.* **2002**, *71*, 2286−2289.
(30) Golberg, D.; Bando, Y.; Tang, C.; Zhi, C. Boron nitride nanotubes. *Adv. Mater.* **2007**, *19*, 2413−2432.
(31) Stewart, D. A.; Savic, I.; Mingo, N. First-principles calculation of the isotope effect on boron nitride nanotube thermal conductivity. *Nano Lett.* **2009**, *9*, 81−84.
(32) Li, T.; Tang, Z.; Huang, Z.; Yu, J. A comparison between the mechanical and thermal properties of single-walled carbon nanotubes and boron nitride nanotubes. *Physica E: Low-dimensional Systems and Nanostructures* **2017**, *85*, 137−142.
(33) Ghassemi, H.; Yassar, R. On the mechanical behavior of boron nitride nanotubes. *Applied Mechanics Reviews* **2010**, *63*, 0804 DOI: 10.1115/1.4001117.
(34) Charlier, J.-C.; Ebbesen, T.; Lambin, P. Structural and electronic properties of pentagon-heptagon pair defects in carbon nanotubes. *Phys. Rev. B* **1996**, *53*, 11108.
(35) Gao, F.; Qu, J.; Yao, M. Effects of local structural defects on the electron transport in a carbon nanotube between Cu electrodes. *Appl. Phys. Lett.* **2010**, *97*, 242112.

(36) Teichert, F.; Zienert, A.; Schuster, J.; Schreiber, M. Electronic transport in metallic carbon nanotubes with mixed defects within the strong localization regime. *Comput. Mater. Sci.* **2017**, *138*, 49−57.
(37) Teichert, F.; Wagner, C.; Croy, A.; Schuster, J. Influence of defect-induced deformations on electron transport in carbon nanotubes. *Journal of Physics Communications* **2018**, *2*, 115023.
(38) Algharagholy, L. A. Defects in carbon nanotubes and their impact on the electronic transport properties. *J. Electron. Mater.* **2019**, *48*, 2301−2306.
(39) Serhan, M.; Abusini, M.; Almahmoud, E.; Omari, R.; Al-Khaza'leh, K.; Abu-Farsakh, H.; Ghozlan, A.; Talla, J. The electronic properties of different chiralities of defected boron nitride nanotubes: theoretical study. *Computational Condensed Matter* **2020**, *22*, e00439.
(40) Kang, H. S. Theoretical study of boron nitride nanotubes with defects in nitrogen-rich synthesis. *J. Phys. Chem. B* **2006**, *110*, 4621−4628.
(41) Kundalwal, S.; Choyal, V. Enhancing the piezoelectric properties of boron nitride nanotubes through defect engineering. *Physica E: Low-dimensional Systems and Nanostructures* **2021**, *125*, 114304.
(42) Collins, P. G. *Defects and disorder in carbon nanotubes*; Oxford University Press: Oxford, 2010.
(43) Abuokaz, M.; Al-khaza'leh, K.; Talla, J. A. Influence of Stone−Wales defects on the structural and electronic properties of double-walled boron nitride nanotubes: density functional theory. *Appl. Phys. A: Mater. Sci. Process.* **2022**, *128*, 1−10.
(44) Geetha, R.; Gayathri, V. Comparative study on gas adsorption in defected carbon and boron nitride nanotube. *Current Nanoscience* **2010**, *6*, 131−136.
(45) Anoop Krishnan, N.; Ghosh, D. Defect induced plasticity and failure mechanism of boron nitride nanotubes under tension. *J. Appl. Phys.* **2014**, *116*, 044313.
(46) Zhi, C.; Bando, Y.; Tang, C.; Golberg, D. Boron nitride nanotubes. *Materials Science and Engineering: R: Reports* **2010**, *70*, 92−111.
(47) Dumitrică, T.; Bettinger, H. F.; Scuseria, G. E.; Yakobson, B. I. Thermodynamics of yield in boron nitride nanotubes. *Phys. Rev. B* **2003**, *68*, 085412.
(48) Chen, Y. K.; Liu, L. V.; Wang, Y. A. Density functional study of interaction of atomic Pt with Pristine and Stone− Wales-defective single-walled boron nitride nanotubes. *J. Phys. Chem. C* **2010**, *114*, 12382−12388.
(49) Krasheninnikov, A.; Nordlund, K. Stability of irradiation-induced point defects on walls of carbon nanotubes. *Journal of Vacuum Science & Technology B: Microelectronics and Nanometer Structures Processing, Measurement, and Phenomena* **2002**, *20*, 728−733.
(50) Zhang, C.-L.; Shen, H.-S. Self-healing in defective carbon nanotubes: a molecular dynamics study. *J. Phys.: Condens. Matter* **2007**, *19*, 386212.
(51) Chegel, R. Tuning electronic properties of carbon nanotubes by Boron and Nitrogen doping. *Physica B: Condensed Matter* **2016**, *499*, 1−16.
(52) Algharagholy, L. A.; Sadeghi, H.; Al-Backri, A. A. Selective sensing of 2, 4, 6-trinitrotoluene and triacetone triperoxide using carbon/boron nitride heteronanotubes. *Materials Today Communications* **2021**, *28*, 102739.
(53) Scardamaglia, M.; Struzzi, C.; Aparicio Rebollo, F. J.; De Marco, P.; Mudimela, P. R.; Colomer, J.-F.; Amati, M.; Gregoratti, L.; Petaccia, L.; Snyders, R.; Bittencourt, C. Tuning electronic properties of carbon nanotubes by nitrogen grafting: Chemistry and chemical stability. *Carbon* **2015**, *83*, 118−127.
(54) Blase, X.; Charlier, J.-C.; De Vita, A.; Car, R. Structural and electronic properties of composite BxCyNz nanotubes and heterojunctions. *Appl. Phys. A: Mater. Sci. Process.* **1999**, *68*, 293−300.
(55) Algharagholy, L.; Pope, T.; Bailey, S. W.; Lambert, C. J. Electronic properties of sculpturenes. *New J. Phys.* **2014**, *16*, 013060.
(56) Chen, L.-N.; Ma, S.-S.; OuYang, F.-P.; Xiao, J.; Xu, H. First-principles study of metallic carbon nanotubes with boron/nitrogen co-doping. *Chinese Physics B* **2011**, *20*, 017103.
(57) Saikia, N.; Deka, R. C. First principles study on the boron−nitrogen domains segregated within (5, 5) and (8, 0) single-wall carbon nanotubes: formation energy, electronic structure and reactivity. *Computational and Theoretical Chemistry* **2012**, *996*, 11−20.
(58) McGuire, K.; Gothard, N.; Gai, P.; Dresselhaus, M.; Sumanasekera, G.; Rao, A. Synthesis and Raman characterization of boron-doped single-walled carbon nanotubes. *Carbon* **2005**, *43*, 219−227.
(59) Sawant, S. V.; Patwardhan, A. W.; Joshi, J. B.; Dasgupta, K. Boron doped carbon nanotubes: Synthesis, characterization and emerging applications−A review. *Chemical Engineering Journal* **2022**, *427*, 131616.
(60) Villalpando-Paez, F.; Zamudio, A.; Elias, A.; Son, H.; Barros, E.; Chou, S.; Kim, Y.; Muramatsu, H.; Hayashi, T.; Kong, J. Synthesis and characterization of long strands of nitrogen-doped single-walled carbon nanotubes. *Chem. Phys. Lett.* **2006**, *424*, 345−352.
(61) Ibrahim, E.; Khavrus, V. O.; Leonhardt, A.; Hampel, S.; Oswald, S.; Rümmeli, M. H.; Büchner, B. Synthesis, characterization, and electrical properties of nitrogen-doped single-walled carbon nanotubes with different nitrogen content. *Diamond and related materials* **2010**, *19*, 1199−1206.
(62) Stephan, O.; Ajayan, P.; Colliex, C.; Redlich, P.; Lambert, J.; Bernier, P.; Lefin, P. Doping graphitic and carbon nanotube structures with boron and nitrogen. *Science* **1994**, *266*, 1683−1685.
(63) Redlich, P.; Loeffler, J.; Ajayan, P.; Bill, J.; Aldinger, F.; Rühle, M. B— C— N nanotubes and boron doping of carbon nanotubes. *Chemical physics letters* **1996**, *260*, 465−470.
(64) Algharagholy, L.; Bailey, S. W.; Pope, T.; Lambert, C. J. Sculpting molecular structures from bilayer graphene and other materials. *Phys. Rev. B* **2012**, *86*, 075427.
(65) Blase, X.; Charlier, J.-C.; De Vita, A.; Car, R. Theory of composite B x C y N z nanotube heterojunctions. *Appl. Phys. Lett.* **1997**, *70*, 197−199.
(66) Algharagholy, L.; Pope, T.; Al-Galiby, Q.; Sadeghi, H.; Bailey, S. W.; Lambert, C. J. Sensing single molecules with carbon−boron-nitride nanotubes. *Journal of Materials Chemistry C* **2015**, *3*, 10273−10276.
(67) Suenaga, K.; Colliex, C.; Demoncy, N.; Loiseau, A.; Pascard, H.; Willaime, F. Synthesis of nanoparticles and nanotubes with well-separated layers of boron nitride and carbon. *Science* **1997**, *278*, 653−655.
(68) Iyyamperumal, E.; Wang, S.; Dai, L. Vertically aligned BCN nanotubes with high capacitance. *ACS Nano* **2012**, *6*, 5259−5265.
(69) Wang, W. L.; Bai, X. D.; Liu, K. H.; Xu, Z.; Golberg, D.; Bando, Y.; Wang, E. G. Direct Synthesis of B−C−N Single-Walled Nanotubes by Bias-Assisted Hot Filament Chemical Vapor Deposition. *J. Am. Chem. Soc.* **2006**, *128*, 6530−6531.
(70) Enouz, S.; Stéphan, O.; Cochon, J.-L.; Colliex, C.; Loiseau, A. C− BN patterned single-walled nanotubes synthesized by laser vaporization. *Nano Lett.* **2007**, *7*, 1856−1862.
(71) Wei, X.; Wang, M.-S.; Bando, Y.; Golberg, D. Electron-beam-induced substitutional carbon doping of boron nitride nanosheets, nanoribbons, and nanotubes. *ACS Nano* **2011**, *5*, 2916−2922.
(72) Yap, Y. K. *Hetero-junctions of boron nitride and carbon nanotubes: Synthesis and characterization*; Michigan Technological University, 2013. DOI: 10.2172/1068533.
(73) Soler, J. M.; Artacho, E.; Gale, J. D.; García, A.; Junquera, J.; Ordejón, P.; Sánchez-Portal, D. The SIESTA method for ab initio order-N materials simulation. *J. Phys.: Condens. Matter* **2002**, *14*, 2745.
(74) Ceperley, D. M.; Alder, B. J. Ground state of the electron gas by a stochastic method. *Physical review letters* **1980**, *45*, 566.
(75) Björkman, T.; Gulans, A.; Krasheninnikov, A.; Nieminen, R. Are we van der Waals ready? *J. Phys.: Condens. Matter* **2012**, *24*, 424218.
(76) Ferrer, J.; Lambert, C. J.; García-Suárez, V. M.; Manrique, D. Z.; Visontai, D.; Oroszlany, L.; Rodríguez-Ferradás, R.; Grace, I.;

https://doi.org/10.1021/acs.jpclett.3c00004
J. Phys. Chem. Lett. 2023, 14, 2056−2064

Bailey, S.; Gillemot, K. GOLLUM: a next-generation simulation tool for electron, thermal and spin transport. *New J. Phys.* **2014**, *16*, 093029.
(77) Chico, L.; Benedict, L. X.; Louie, S. G.; Cohen, M. L. Quantum conductance of carbon nanotubes with defects. *Phys. Rev. B* **1996**, *54*, 2600.
(78) Lambin, P.; Fonseca, A.; Vigneron, J.-P.; Nagy, J. B.; Lucas, A. Structural and electronic properties of bent carbon nanotubes. *Chem. Phys. Lett.* **1995**, *245*, 85−89.
(79) Zhang, M.; Li, J. Carbon nanotube in different shapes. *Mater. Today* **2009**, *12*, 12−18.
(80) Srivastava, D.; Menon, M. Structure of Boron Nitride Nanotubes: Tube Closing Vs. Chirality. *Chem. Phys. Lett.* **1999**, 407.
(81) Ghassemi, H. M.; Lee, C. H.; Yap, Y. K.; Yassar, R. S. Field emission and strain engineering of electronic properties in boron nitride nanotubes. *Nanotechnology* **2012**, *23*, 105702.
(82) Cheng, G.; Yao, S.; Sang, X.; Hao, B.; Zhang, D.; Yap, Y. K.; Zhu, Y. Evolution of Irradiation-Induced Vacancy Defects in Boron Nitride Nanotubes. *Small* **2016**, *12*, 818−824.
(83) Bai, X.; Golberg, D.; Bando, Y.; Zhi, C.; Tang, C.; Mitome, M.; Kurashima, K. Deformation-driven electrical transport of individual boron nitride nanotubes. *Nano Lett.* **2007**, *7*, 632−637.
(84) Buongiorno Nardelli, M.; Brabec, C.; Maiti, A.; Roland, C.; Bernholc, J. Lip-lip interactions and the growth of multiwalled carbon nanotubes. *Physical review letters* **1998**, *80*, 313.
(85) Meunier, V.; Henrard, L.; Lambin, P. Energetics of bent carbon nanotubes. *Phys. Rev. B* **1998**, *57*, 2586.
(86) Srivastava, D.; Brenner, D. W.; Schall, J. D.; Ausman, K. D.; Yu, M.; Ruoff, R. S. Predictions of enhanced chemical reactivity at regions of local conformational strain on carbon nanotubes: kinky chemistry. *J. Phys. Chem. B* **1999**, *103*, 4330−4337.
(87) Han, J.; Anantram, M.; Jaffe, R.; Kong, J.; Dai, H. Observation and modeling of single-wall carbon nanotube bend junctions. *Phys. Rev. B* **1998**, *57*, 14983.
(88) Venema, L.; Janssen, J.; Buitelaar, M.; Wildöer, J.; Lemay, S.; Kouwenhoven, L.; Dekker, C. Spatially resolved scanning tunneling spectroscopy on single-walled carbon nanotubes. *Phys. Rev. B* **2000**, *62*, 5238.
(89) Ghassemi, H. M.; Lee, C. H.; Yap, Y. K.; Yassar, R. S. In situ observation of reversible rippling in multi-walled boron nitride nanotubes. *Nanotechnology* **2011**, *22*, 115702.
(90) Terrones, M.; Romo-Herrera, J.; Cruz-Silva, E.; López-Urías, F.; Munoz-Sandoval, E.; Velázquez-Salazar, J.; Terrones, H.; Bando, Y.; Golberg, D. Pure and doped boron nitride nanotubes. *Mater. Today* **2007**, *10*, 30−38.
(91) Sadeghi, H. Theory of electron, phonon and spin transport in nanoscale quantum devices. *Nanotechnology* **2018**, *29*, 373001.

https://doi.org/10.1021/acs.jpclett.3c00004
J. Phys. Chem. Lett. 2023, 14, 2056−2064